Marie Chilton, originally from Richland, WA, is a sophomore at Brigham Young University majoring in Mathematics and Chemistry. She participated in the Young Women in Science internship at Pacific Northwest National Laboratory for two years before her work there in the summer of 2008 under the SULI program. Marie is currently working with Dr. Jaron Hansen and Dr. Lee Hansen at Brigham Young University on research using calorimetry to determine rate constants and enthalpy changes.

Stephen J. Walsh is a research scientist at Pacific Northwest National Laboratory in Richland WA. He holds an M.S. in Statistics from Montana State University (2007) and a B.S. in Mathematics from Montana Tech of the University of Montana (2004). Dr. Walsh has worked in remote sensing, quality control, seismology, geology and the social sciences. His research has focused on the application of statistical theory to problems in remote sensing.

Don Simone Daly is a senior research scientist at the Pacific Northwest National Laboratory in Richland WA. He received his Ph.D. in statistics from the Montana State University in 1997. With his extensive undergraduate training in chemistry, physics and electrical and mechanical engineering, Dr. Daly has applied statistical thinking in a wide variety of scientific and engineering domains including materials science, molecular biology, non-destructive evaluation and remote sensing. His research has focused on instrument modeling and the role of statistics in the execution of the scientific method.

Prediction Metrics for Chemical Detection in Long-Wave Infrared Hyperspectral Imagery

Marie Chilton, Stephen J. Walsh and Don S. Daly

ABSTRACT

Natural and man-made chemical processes generate gaseous plumes that may be detected by hyperspectral imaging, which produces a matrix of spectra affected by the chemical constituents of the plume, the atmosphere, the bounding background surface and instrument noise. A physics-based model of observed radiance shows that high chemical absorbance and low background emissivity result in a larger chemical signature. Using simulated hyperspectral imagery, this study investigated two metrics which exploited this relationship. The objective was to explore how well the chosen metrics predicted when a chemical would be more easily detected when comparing one background type to another. The two predictor metrics correctly rank ordered the backgrounds for about 94% of the chemicals tested as compared to the background rank orders from Whitened Matched Filtering (a detection algorithm) of the simulated spectra. These results suggest that the metrics provide a reasonable summary of how the background emissivity and chemical absorbance interact to produce the at-sensor chemical signal. This study suggests that similarly effective predictors that account for more general physical conditions may be derived.

Introduction

Agricultural, manufacturing and natural chemical processes can generate characteristic gaseous plumes. Nearly every molecular gas has a unique long-wave infrared (LWIR) absorption spectrum. Thus chemical constituents of gaseous plumes can be detected and identified in LWIR hyperspectral images [1]. Chemical detectability depends upon many nuisance factors such as the background type. It may be possible to predict the relative detectability of a chemical as a function of such nuisance factors.

Hyperspectral sensors collect a three-dimensional array of radiance observations. The observed ground area accounts for two dimensions of this image. The third dimension is defined by a wavenumber range of the electromagnetic spectrum. A radiance measurement is the sum of the cumulative effects of the plume gas type, plume gas concentration, atmosphere, background surface, temperature difference between the plume and background, and instrument noise [1], [2].

Plume detection and characterization is a complex problem. Real-world data that lends itself to understanding the physical phenomenology is almost non-existent. As such, this study uses computer simulations to explore the relationship between the effects of background surface and gas type on the detectability of 499 gases over six distinct backgrounds. The simulated data is produced by a physics-based model. Chemical detections are decided by a Whitened Matched Filter (a detection algorithm) [1]. The objective of this research is to evaluate predictors of relative chemical detectability that are functions of laboratory chemical absorbance and background spectra.

Introduction to the Physics of Radiative Transfer

Sensor-observed radiance can be summarized by a physics-based model that incorporates the effects of the plume gas, background surface, temperature difference between the plume and the ground, and the atmosphere recorded radiance [2]. According to Kirchoff's law, all incident radiation is reflected, absorbed or transmitted by the body it impacts, or $1 = \alpha + \tau + \rho$, where α is the fraction of radiation the body absorbs, τ is the fraction of radiation the body transmits, and ρ is the fraction of radiation the body reflects [3].

Further, Kirchoff's law states that at thermodynamic equilibrium, an object's absorbance is equal to its emissivity *(ε)* defined as the proportion of radiation an object emits to the radiation it would emit as a blackbody at the same temperature. Since a blackbody is an object which absorbs and emits all incident radiation and since no natural object is a perfect blackbody, $0 < \varepsilon < 1$ [2].

For optically thin plumes, the transmissivity of the plume (τ_p) can be reasonably approximated by $1 - A(\nu) \cdot c$ for small c where $A(\nu)$ is the chemical absorbance in inverse parts-per-million-meter denoted $(\text{ppm-m})^{-1}$ at wavenumber $\nu(\text{cm}^{-1})$ and c is the concentration path length of the gas measured in ppm-m [2]. The expression for radiance recorded by the instrument with a plume present, L_{obs}, can be expressed as the sum of noise and the signal due to each of three layers: plume, ground and atmosphere. Explicitly:

$$L_{obs}(\nu) = \tau_a(\nu)[B(T_p;\nu) - L_g(\nu)] \cdot A(\nu) \cdot c + \tau_a(\nu) L_g(\nu) + L_u(\nu) + e(\nu), \quad (1)$$

is the physics-based model for L_{obs} as a function of wavenumber, ν, where $\tau_a(\nu)$ is the transmissivity of the atmosphere at ν; $B(T_p;\nu)$ $(\text{W/cm}^2/\text{Sr/cm}^{-1})$ is Planck's Blackbody function for radiance at plume temperature T_p(K) and wavenumber ν; $L_g(\nu)$ is the radiance due to the background surface; $L_u(\nu)$ is the atmospheric up-welling radiance; and $e(\nu)$ represents measurement and modeling error. A graphical representation of Eq. (1) is presented in Figure 1 [2]. The background radiance $L_g(\nu)$ may be expressed as

$$L_g(\nu) = \varepsilon_g(\nu) B(T_g;\nu), \quad (2)$$

where ε_g is the emissivity of the ground [2]. Note that this expression ignores reflected down-welling radiance because its impact on L_{obs} is negligible [3].

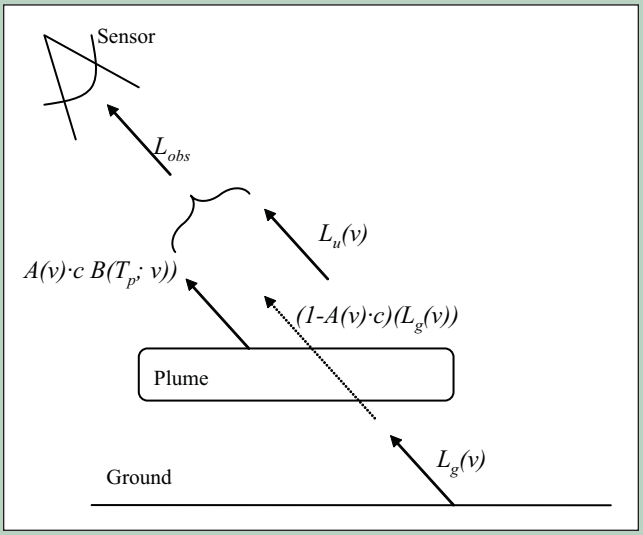

Figure 1. Graphical representation of the observed radiance equation. The ground radiance $L_g(\nu)$ is filtered by the plume with radiance $A(\nu)\cdot c\ B(T_p;\nu)$ which when combined with the atmospheric radiance $Lu(\nu)$ is observed as L_{obs}.

Plume/Ground Temperature Equality

For this paper we studied an admittedly constraining plume/ground temperature case. The intent was to remove the effect of the plume/ground temperature difference on the chemical signal in order to isolate the interaction between background emissivity and chemical absorbance. More general temperature cases may be considered in future work. Setting $T_p = T_g = T$ and substituting Eq. (2) into Eq. (1) yields a simplified expression of the physics-based model that more clearly shows the relationship between background emissivity and chemical absorbance:

$$L_{obs}(\nu) = \tau_a(\nu)[B(T;\nu)][1 - \varepsilon_g(\nu)] \cdot A(\nu) \cdot c + \tau_a(\nu) L_g(\nu) + L_u(\nu) + e(\nu). \quad (3)$$

Note that the signal due to the chemical effluent is the first term on the right hand side of Eq. (3), explicitly:

$$\tau_a(\nu)[B(T;\nu)][1 - \varepsilon_g(\nu)] A(\nu) \cdot c. \quad (4)$$

Expression (4) shows that a relatively larger gas absorbance, $A(\nu)$, and a background emissivity, $\varepsilon_g(\nu)$, close to 0 (or, equivalently a background reflectance, $1 - \varepsilon_g(\nu)$, close to 1) contribute to a relatively larger chemical signal in $L_{obs}(\nu)$ and in turn to relatively higher gas detection probability. We used this reasoning to produce summary measures using chemical absorbance and background emissivity.

Predictors

Based on the intuition gained from the physics-based model, two predictors were explored for their ability to summarize when a chemical may be better detected over one background type versus another. One predictor (M_1) uses each background's reflectance $(1 - \varepsilon_g)$ at the wavenumber where the absolute maximum chemical absorbance occurs to rank order backgrounds, i.e.

$$M_1 = 1 - \varepsilon_g(\nu^*) \text{ where } \nu^* = \arg\max_\nu A(\nu). \quad (5)$$

Eq. (3) suggests that the background with the largest M_1 for a given chemical will yield the largest $L_{obs}(\nu^*)$. The dominance of the maximum gas absorbance on detection for a given background is explored with this metric.

Though the chemical absorbance is approximately zero at most wavenumbers, many chemicals may have multiple relative maxima where $\varepsilon_g(\nu)$ is also low and these also contribute to the radiance spectrum recorded by the instrument. As such, a predictor that accounts for the chemical absorbance and background emissivity across the whole spectrum is also explored. This predictor sums the products of the squared chemical absorbance and squared background reflectance at each observed wavenumber in the LWIR. It also normalizes the given chemical absorbance spectrum by dividing by its squared magnitude. This predictor is denoted M_2 and is given by:

$$M_2 = \frac{\sum_{i=1}^{n} (A_i)^2 (1 - \varepsilon_{g_i})^2}{\sum_{i=1}^{n} (A_i)^2}, \quad (6)$$

where n represents the number of wavenumbers (or number of observed spectral channels). Chemical absorbances and background emissivities that generally contribute to larger $L_{obs}(\nu)$ over all wavenumbers tend to give larger values of M_2.

As an example of how M_1 and M_2 would rank order backgrounds for a specific chemical, the chemical absorbance spectrum of carbon tetrachloride (CCl_4) using the background emissivity spectra of a Paint representative and an Asphalt-Concrete-Soil representative (ACS) are plotted in Figure 2. The absolute maximum of CCl_4 occurs at wavenumber 794 and at that wavenumber, Paint has a greater reflectance ($1-\varepsilon_g$) than ACS so M_1 would order the backgrounds as Paint and then ACS for CCl_4. Similarly, M_2 for CCl_4 and Paint is 7.499×10^{-3} while M_2 for CCl_4 and ACS is 1.689×10^{-3}. Thus M_2 would also order these backgrounds as Paint and then ACS for CCl_4. The background orderings as decided by these predictors will be compared to the actual background orderings as decided by a commonly applied chemical detection algorithm.

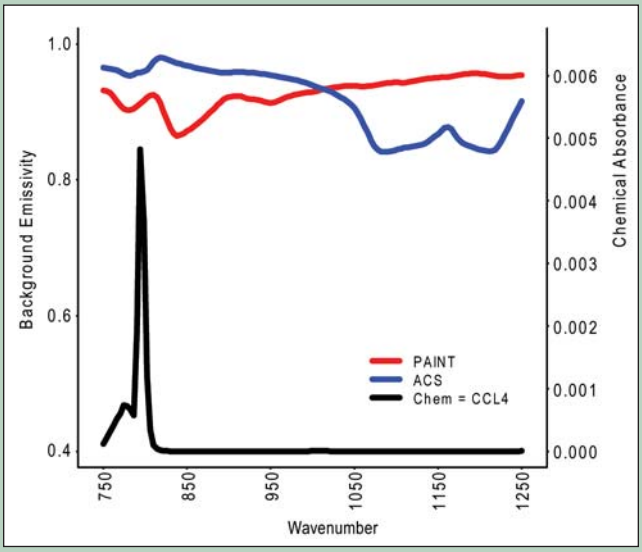

Figure 2. Chemical absorbance spectrum of CCl_4 with PAINT and ACS background emissivity spectra. The difference between PAINT and ACS over the wavenumbers with highest CCl_4 absorbance predicts that CCl_4 would be more easily detected over PAINT then ACS.

Both predictors focus on chemical absorbance and background emissivity, assuming the other variables in the physics-based model, Eq. (3), are held constant. In actual and simulated hyperspectral images, the other variables and noise can also perturb gas detectability. Future work may consider more general plume/ground temperature cases as well as incorporating the atmospheric transmissivity in more generalized predictors.

Methods

It would be ideal to generate hyperspectral images in the natural environment where all variables could be controlled and manipulated to compare relative detectability of various chemicals over specific backgrounds. However, since this level of control would be extremely difficult and costly (or unattainable) in a real experiment, analysis of computer-simulated data was conducted instead. This allows the relationship between chemical absorbance and background emissivity to be better understood, especially as it relates to gas detectability. We do this by comparing detection results on the simulated hyperspectra to the background orderings as decided by M_1 and M_2.

This experiment used the InfraRed Systems Analysis in General Environments code (IR-SAGE) developed at Pacific Northwest National Laboratory (PNNL) [4] to simulate LWIR hyperspectra of simplified gaseous plumes over organized background pixels. IR-SAGE uses the physics-based model in Eq. (1) to simulate a radiance vector from the LWIR using a chemical absorbance spectrum, a background emissivity spectrum and atmospheric conditions, while perturbing these quantities with Gaussian noise [4]. Gas absorbance spectra from the PNNL library [6] were used for image simulation. Background emissivity spectra used in the IR-SAGE images were selected from the Nonconventional Exploitation Factors Data System (NEFDS) [7]. Six distinct background emissivities were chosen for image simulation. These emissivities exhibit different behavior across the LWIR spectrum.

One 36-part data cube was simulated for the 499 distinct gases in the library. For all images, the temperature of the plume was set equal to the temperature of the ground so that $T_p = T_g = 300K$. The spectral range used was 750 to 1250 cm^{-1} in steps of four which yielded a total of 126 spectral channels. Each 36-part cube had dimensions of $150 \times 120 \times 126$ (rows by columns by spectral channels). Each set of 25 rows represented one of the six distinct background types: Asphalt-Concrete-Soil (ACS), Brick, Miscellaneous (MSC), Paint, Snow and Steel and Copper tubing (STCOP). Each set of 20 columns corresponded to a different gas concentration path-length: 16, 8, 4, 2, 1 and 0 ppm-m. Thus each $25 \times 20 \times 126$ part contained 500 replicate pixels for one of the 36 background/gas concentration combinations.

We used a Whitened Matched Filter (WMF) as the gas detection tool [1]. Radiance due to background was first removed from a plume pixel by computing the mean of all ppm-m concentration pixels and then subtracting it from the plume radiance:

$$L_W = L_{on} - L_{off}. \quad (7)$$

Here, L_W, L_{on} and L_{off} are radiance vectors of length 126. Therefore, L_{on} represents a plume pixel and L_w represents the radiance due to the plume and noise after removing the background radiance. These "whitened" spectra were then processed with the WMF. The expression for the scalar WMF can be written as

$$WMF = (A' \hat{\Sigma}^{-1} A)^{-1} A' \hat{\Sigma}^{-1} L_W, \quad (8)$$

where A is the chemical absorbance spectrum (vector of length 126) and $\hat{\Sigma}$ is the covariance matrix of the off-plume pixels with dimensions 126×126. Eq. (8) emphasizes the strength of the chemical signal in L_w while diminishing the effects of noise through the use of $\hat{\Sigma}^{-1}$. In practice, large values of the WMF provide evidence for gas detection [2]. The filter was applied to each pixel. It was necessary to pick a threshold in order to label a pixel as a chemical detection or non-detection. Thus a gas was "detected" in a pixel if WMF was statistically different from zero at the 0.05 significance level [5]. The proportion of gas detections, denoted by $\hat{p}$, out of the 500 replicate pixels was used as an estimate of the gas detection probability for each background type. Backgrounds were ordered for each chemical based on these $\hat{p}$ values. An example of a detection proportion curve for the CCl_4 image is presented in Figure 3. The detection proportions are plotted as a function of gas concentration path-length. There is one $\hat{p}$ curve for each of the six backgrounds. This plot indicates that CCl_4 was best detected over Paint and

worst detected over Snow. The data presented in Figure 3 is used to order the backgrounds for best-to-worst detectability of CCl_4. This plot gives the ordering as: Paint, STCOP, MSC, Brick, ACS and Snow. Recall the previous examples of predictor metrics. For CCl_4, M_1 and M_2 both ordered two of the backgrounds as Paint and then ACS. We note that these background orderings correspond to the relative ordering of Paint and ACS for CCl_4 as decided by the WMF detections.

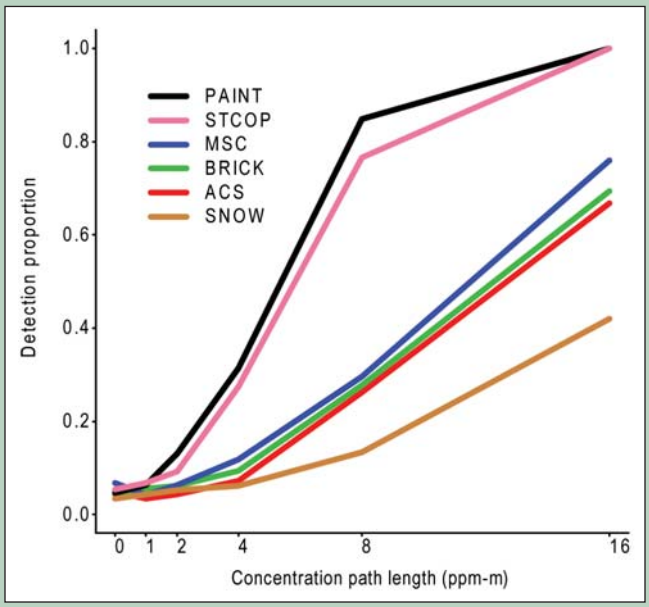

Figure 3. Example detection proportion curves from simulated image of CCl_4 plume. In the simulation, CCl_4 was more easily detected using WMF over PAINT, than STCOP, MSC, BRICK, ACS and finally SNOW, respectively.

Metrics M_1 and M_2 were calculated for all chemical/background combinations using the chemical absorbance spectra from the PNNL gas library and the six aforementioned background emissivity spectra. These metrics gave a ranking of the background types for each chemical. Recall that the physics-based model indicates that, for a given chemical, backgrounds that yield relatively larger scores for M_1 and M_2 will tend to yield relatively larger chemical signals and hence relatively higher detection proportions. Thus for a given chemical, the background orderings as indicated by $\hat{p}$, M_1 and M_2 were interrogated for consistency. We interpret high consistency in these rank orderings as an indication that M_1 and M_2 provide reasonable summaries of how gas absorbance and background emissivity interact to produce the at-sensor observed chemical signal and in turn provide good predictive ability to describe when a chemical will be more easily detected over one background as compared to another.

Results and Discussion

Initial inspection of the detection results using the Whitened Matched Filter for the 499 images revealed that 276 chemicals had $\hat{p}$ values less than 0.2 across all backgrounds and concentrations. For these chemicals, the detection proportion curves were not separated enough to decide how the backgrounds should be rank ordered. This was attributed to a relatively low and flat chemical absorbance across the LWIR (relative to the chemicals that gave overall large detections). These gases would require simulations that used larger concentration path lengths than those considered to produce informative detection curves. As such, these gases were removed from the study.

For the remaining 223 chemicals, the consistency in background rank orderings among $\hat{p}$, M_1 and M_2 is summarized in Figure 4. Results are shown in a composite bar chart that displays the proportion of rankings that agreed for all three measures (blue), the proportion of rankings that agreed between $\hat{p}$ and M_1 only (yellow), the proportion of rankings that agreed between $\hat{p}$ and M_2 only (orange) and the proportion of rankings that did not agree among all three measures (red). The chart in Figure 4 indicates that M_1 and M_2 were each able to correctly rank order the backgrounds (as compared to the rankings decided by $\hat{p}$) for over 90% of the chemicals. Comparison of the yellow and orange regions of the bars indicates marginal difference in the abilities of M_1 and M_2 to correctly rank order the backgrounds. These results indicate that both M_1 and M_2 are competitive predictors for when a chemical will be better detected over one background type or another. These results hold only for these data and the assumptions we have applied to the physics-based model.

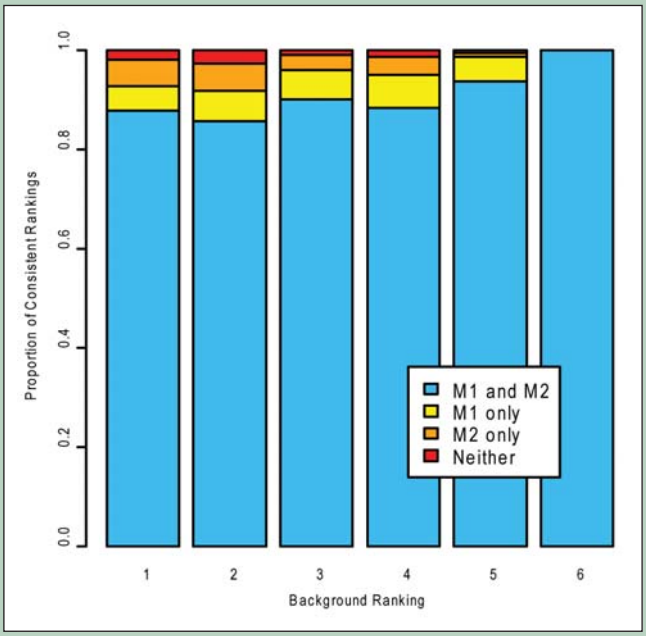

Figure 4. The distribution of agreement among $\hat{p}$, M_1 and M_2 in background rankings. The blue denotes the proportion of chemicals for which the background rank agreed between all measures. The yellow and orange indicate the proportion of chemicals for which the background rank agreed between $\hat{p}$ and M_1 only, or between $\hat{p}$ and M_2 only, respectively. The red denotes when the background ranking disagreed across $\hat{p}$, M_1 and M.

Conclusion

Based on the physics-based model, high chemical absorbance and low background emissivity contribute to high gas detectability assuming other variables and noise are held constant. Two predictors were developed to investigate the implications of the physics-based model: one predictor accounted for chemical absorbance and background emissivity at a single wavenumber and the other predictor accounted for these properties across the LWIR spectrum.

Backgrounds were rank ordered based on these predictors for each chemical and compared with the background ordering for gas detection from simulated experimental results.

Simulating and analyzing all 499 data cubes took approximately 72 cpu hours and introduced computational problems because of the size and complexity of each file. Additional sets of data cubes for different conditions would have required too great an amount of cpu time to analyze. These time constraints limited our study to the one plume/ground temperature case: $T_p = T_g$. Plots of chemical absorbance spectra compared to their $\hat{p}$ values suggest that the low magnitude of absorbance spectra was a factor in preventing the other 276 chemicals from being detected in this simulation. This suggests that many of these chemicals would be detectable at higher concentrations. This was not further explored due to time constraints.

Alone, M_1 and M_2 each correctly rank ordered the backgrounds for more than 90% of the 223 chemicals. Even though M_1 focuses only on the chemical absorbance and background emissivity at a single wavenumber, M_1 and M_2 yield similar results. However, M_1 is much simpler computationally and thus it may be considered a better summary metric for these data.

These results are encouraging and suggest that M_1 and M_2 adequately summarize how the background emissivity and chemical absorbance work in conjunction to produce the chemical signal and are good predictors for when a chemical may be better detected over one background type as to another. Future work will attempt to generalize M_1 and M_2 with the aim of incorporating other physics-based parameters and a wider set of conditions on the plume/ground temperatures.

Acknowledgements

We thank Mark Tardiff and Dr. Candace Metoyer for their advice and support. This work was made possible by the U.S. Department of Energy (DOE), Office of Science through the Science Undergraduate Laboratory Internship program. Additional support was provided by the PNNL operated by Battelle for DOE under Contract DE-AC06-76RL01830.

References

[1] D. Messinger, C. Salvaggio and N. Sinisgalli, "Detection of gaseous effluents from airborne LWIR hyperspectral imagery using physics-based signatures," *International Journal of High Speed Electronics and Systems*, vol. 17, no. 6, pp. 801–812, 2006.

[2] T. Burr and N. Hengartner, "Overview of physical models and statistical approaches for weak gaseous plume detection using passive infrared hyperspectral imagery," *Sensors*, vol. 6, pp. 1721–1750, 2006.

[3] J. Schott, *Remote Sensing*, New York: Oxford Press, 1997.

[4] N. Gallagher, D. Sheen, J. Shaver, B. Wise and J. Shultz, "Estimation of trace vapor concentration path-length in plumes for remote sensing applications from hyperspectral images," *Proceedings of the SPIE*, vol. 5093, pp. 184–194, 2003.

[5] J. Neter, M. Kutner, C. Nachtsheim and W. Wasserman, *Applied Linear Statistical Models*, 4th ed. Boston: McGraw-Hill, 1996.

[6] S.W. Sharpe, T.J. Johnson, R.L. Sams, P.M. Chu, G.C. Rhoderick and P.A. Johnson, "Gas-Phase Databases for Quantitative Infrared Spectroscopy," *Applied Spectroscopy*, vol. 58, pp. 1452–1461, 2004.

[7] H.B. Westlund and G.W. Meyer, "A BRDF database employing the Beard-Maxwell reflection model," *Proceedings of Graphics Interface*, 2002.